SUPPLEMENT TO THE *WELDING JOURNAL*, FEBRUARY 2013
Sponsored by the American Welding Society and the Welding Research Council

GMA Brazing of Galvannealed Interstitial-Free Steel

A unique process that combines brazing and gas metal arc welding has displayed an ability to reach 100% joint efficiency in thin zinc-coated steel

BY S. BASAK, T. K. PAL, M. SHOME, AND J. MAITY

ABSTRACT

The gas metal arc (GMA) brazing process (a novel approach that combines GMA welding and brazing) was applied for joining a new-generation automotive steel (interstitial-free steel) using silicon-containing copper-based filler metal. During this joining process, an interface region of very high hardness was developed through the diffusion of the silicon present in the molten braze metal into the solid steel. The interface microstructure consisted of silicon-enriched, iron-based intermediate phase α_1 for lower heat input and dispersed submicroscopic Fe_5Si_3 particles in α_1 matrix for higher heat input. The calculated diffusion distance of silicon was in excellent agreement with the measured interface width, which envisaged the diffusion of silicon in iron matrix as the controlling factor for evolution of the interface region. The thermodynamic calculations exhibited the lowest Gibbs free-energy change for Fe_5Si_3 as compared to other compounds of Fe and Si to justify the stability of Fe_5Si_3 in the microstructure. Accordingly, during tensile shear tests, the failure occurred in the base metal region, i.e., not at the harder and stronger joint interface. These results suggested a successful joining with 100% joint efficiency.

Introduction

Interstitial-free (IF) steel has been regarded as an important class of new-generation steel where the content of interstitial solute (carbon and nitrogen) is brought down below 50 ppm in order to avoid discontinuous yielding and strain aging (which increases strength at the expense of ductility). This steel, therefore, possesses excellent formability and finds an extensive application in thin-sheet galvannealed (zinc-coated) form in automotive industries for making car bodies (Ref. 1). In general, the joining of zinc-coated thin steel sheets by conventional arc welding processes, such as gas metal arc welding (GMAW), gas tungsten arc welding (GTAW), and others, encounters several difficulties. The main difficulty of arc welding arises due to high arc energy that causes vaporization of the zinc coating. This occurs not only at the joint region but also at a relatively large area around the joint (Refs. 2, 3). Other issues with arc welding include a wider heat-affected zone (HAZ), generation of spatter, risk of melt through, potential contamination, and relatively large residual stress generation and associated distortion (Refs. 3, 4). On the other hand, in automotive industries, the bare steel sheets are efficiently joined by resistance spot welding using a copper electrode. However, for zinc-coated steel sheets, copper electrodes deteriorate quickly through alloying with Zn (Refs. 5–9). This requires frequent replacement of electrodes in resistance spot welding for joining zinc-coated steel sheets. In recent years, in order to overcome such problems a novel combination of GMAW and brazing processes (called GMA brazing) has been proposed where the consumable electrode (usually a copper-based alloy) itself acts as the filler metal that melts and fills the joint clearance between thin steel sheets through capillary action (following the principle of brazing), while the steel sheets remain at solid state since the process is carried out at much lower heat input (Refs. 2, 3). In the process, the zinc coating only vaporizes locally at the joint region. While the joint region is being filled by the copper-based braze alloy, the corrosion resistance and aesthetic appearance are maintained. Melt-through risk, generation of spatter, residual stress, and distortion are reduced due to lower heat input requirements, which also account for energy savings. The main challenge of this process is to achieve adequate joint strength (100% joint efficiency) with the use of a copper-based (nonferrous) filler metal. While joining DP 600 and TRIP 700 steel sheets by GMA brazing process with copper-based filler metals containing Al-Ni and Mn-Al, Chovet and Guiheux (Ref. 3) reported difficulty in obtaining 100% joint efficiency. Moreover, only a few research works have been carried out with regard to the application of this novel process on zinc-coated common steel sheets, which mainly deal with mechanical parameters (Refs. 2–4). The influence of shielding gases and process parameters on metal transfer and bead shape in GMA brazed joints of zinc-coated steel plates has been investigated by Iordachescu et al. (Ref. 4). The short-circuit mode of metal transfer with argon-based gas mixture containing H_2 and He was reported to provide acceptable bead shape and adequate arc stability. However, the in-depth microstructural study with regard to the joining process (phase evolution, thermodynamic stability of phases, etc.) is still pending. Moreover, the application of GMA brazing particularly on IF steel in order to achieve 100% joint efficiency is not

S. BASAK (sushovanbasak@gmail.com) *is senior research fellow and T. K. PAL* (tkpal.ju@gmail.com) *is professor, Metallurgical & Material Engineering Department, Jadavpur University, Kolkata, West Bengal, India. M. SHOME* (mshome@tatasteel.com) *is head, Material Characterization and Joining Research Group, R & D, Tata Steel Ltd., Jamshedpur, Jharkhand, India. J. MAITY* (joydeep_maity@yahoo.com) *is Associate Professor, Department of Metallurgical and Materials Engineering, National Institute of Technology Durgapur, Durgapur, West Bengal, India.*

KEYWORDS

IF Steel
Brazing
Diffusion
α_1 Interface
Dispersed Fe_5Si_3

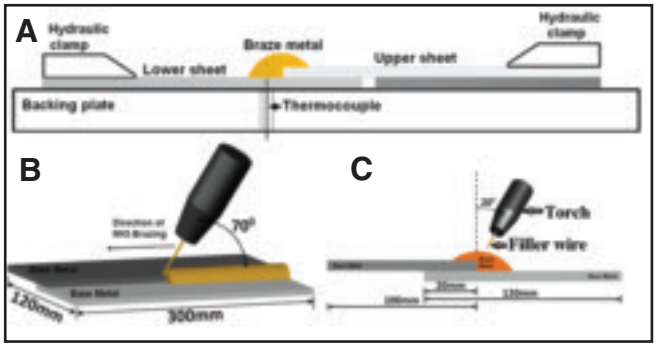

Fig. 1 — Schematic diagram of the GMA brazing process. A — Experimental setup; B — GMA brazing procedure with forehand travel angle; C — with working angle.

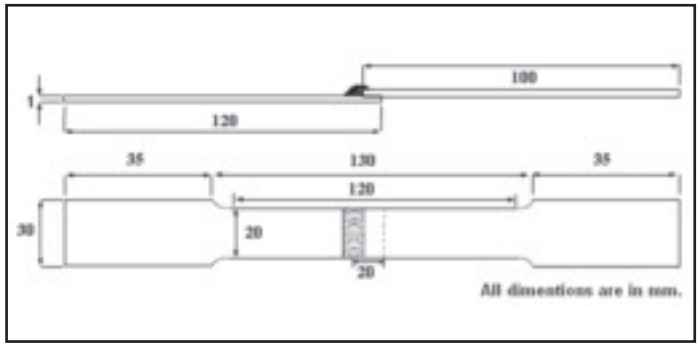

Fig. 2— Schematic diagram of tensile test specimen.

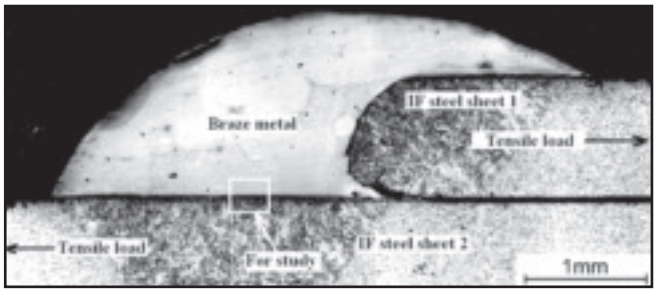

Fig. 3 — Typical macrophotograph of the IF steel sheets joined by GMA brazing process (higher heat input).

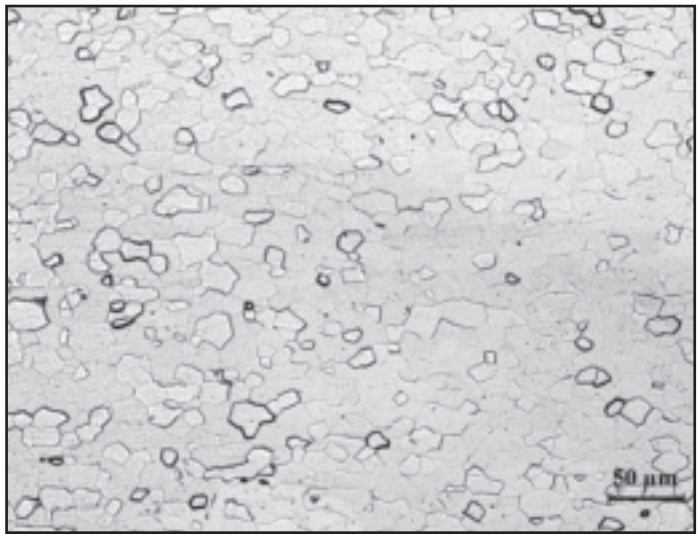

Fig. 4 — Optical microstructure of the unaffected base metal.

readily available as a research report.

In the present research work, the GMA brazing process is applied for joining galvannealed IF steel sheets using silicon- containing copper-based braze alloy to achieve 100% joint efficiency. The detailed process mechanism in view of atomic diffusion and thermodynamic phase stability is analyzed in correlation with phase evolution typically characterized by optical metallography, field emission scanning electron microscopy (FESEM), FESEM-based energy dispersive X-ray spectroscopy (EDS), high resolution transmission electron microscopy (TEM), and TEM-based selected area electron diffraction.

Experimental Procedure

The material for the present investigation is zinc-coated (galvannealed) sheets of interstitial-free steel (Grade: HIF-GA) of 1 mm thickness. The chemical composition of this steel is shown in Table 1. The as-received steel sheets were degreased with acetone and suitably clamped together to form a lap joint. Thereafter, GMA brazing of the lap joint was performed using a pulsed-synergic machine of 270-A capacity (Trans Pulse Synergic 2700 4R/E, Fronius, Austria) with copper-based filler metal (consumable electrode) containing 3.7 wt-% silicon. A schematic experimental setup is shown in Fig. 1. The GMA brazing was carried out at two different heat inputs (considering 70% machine efficiency) with varying current and welding speed as given in Table 2. The torch was traversed automatically along the edge of the upper sheet. The lap joint with a forehand travel angle of about 70 deg and a working angle of 20 deg was maintained. Pure argon was used as the shielding gas at a flow rate of 12 L min^{-1}. During GMA brazing, the temperature profile of the joint region near the interface for the two different heat inputs (specimens P1 and P2) was measured with an R-type (platinum-rhodium) thermocouple of 1.5 mm diameter using a digital temperature recorder (MV1000, Yokogawa, Japan).

After GMA brazing, the small samples were cut from the joint region along the transverse section of the welded sheet for metallographic evaluation. These specimens were polished with successive grades of emery papers up to 1000-grit size followed by cloth polishing with 1-µm diamond paste and thereafter etched with a 2% Nital solution. The metallographic specimens were examined under optical microscope (Zeiss, Imager A1m, Germany), and a FESEM (Zeiss, SUPRA25, Germany) equipped with EDS detector (INCA Penta

Table 1 — Chemical Composition of the IF Steel Sheet (wt-%)

C	Si	Mn	P	Ti	Fe
0.0024	0.094	0.470	0.027	0.035	balance

Table 2 — GMA Brazing Parameters

Specimen Code	Mean Current (A)	Mean Voltage (V)	Wire Feed Speed (mm s^{-1})	Welding Speed (mm s^{-1})	Heat Input (J mm^{-1})
P1	44	16.6	60.00	8.33	61.38
P2	60	18.0	81.67	6.67	113.34

FET, Oxford, UK). Grain size of ferrite in relevant optical images was measured in terms of average grain diameter as per ASTM E112 standard (Ref. 10). The area fractions occupied by relevant phases were measured by standard point count analysis (Ref. 10). In order to identify the different phases present as a whole in the joint region, specimens were subjected to X-ray diffraction (XRD) analysis with slow scan rate (1 deg min^{-1}) in a high-resolution X-ray diffractometer (X' Pert Pro, PANalytical Instruments, Netherlands). Subsequently, thin foils of the specimens were studied under a high-resolution TEM (CM-70, Philips Ltd., Netherlands) equipped with selected area electron diffraction.

Cross sections of the specimens from the joint region were also mounted for microhardness testing. Microhardness measurements were taken at a load of 50 gf along a line perpendicular to the joint interface using a standard microhardness testing machine (AMH43, LECO, U.S.A.). Finally, the lap joint samples were machined to prepare standard tensile-shear test specimens following DIN EN 10002-1 standard (Ref. 11). A schematic diagram of the tensile shear test specimen is shown in Fig. 2. Tensile shear tests were carried out in a 100-kN capacity universal testing machine (Instron-8862, UK) at a crosshead speed of 0.5 mm min^{-1}. The loading direction for tensile shear test is indicated on the macrophotograph of the lap joint — Fig. 3.

Results and Discussion

Microstructural Evolution at the Joint Region

A typical macrophotograph of the IF steel sheets joined by GMA brazing process is shown in Fig. 3. The region of the joint selected for metallographic study is clearly highlighted on the figure. With regard to the microstructural areas of interest, the joint region after GMA brazing of the IF steel have been classified as: 1) unaffected base metal, 2) heat-affected zone (HAZ), 3) interface region, and 4) braze metal. The typical optical microstructure of the unaffected base metal in etched condition is shown in Fig. 4, which is comprised of equiaxed polygonal ferrite grains. The measured grain size of polygonal ferrite is 34 μm.

The FESEM backscattered electron images along with EDS elemental mapping of the joint region are presented in Figs. 5, 6. They depict the overall view of the different significant parts for both the specimens (P1 with lower heat input and P2 with higher heat input) in as-polished (unetched) condition. Furthermore, the EDS line scans of the joint region for P1 and P2 are shown in Fig. 7. The optical microstructures of the HAZ region of the

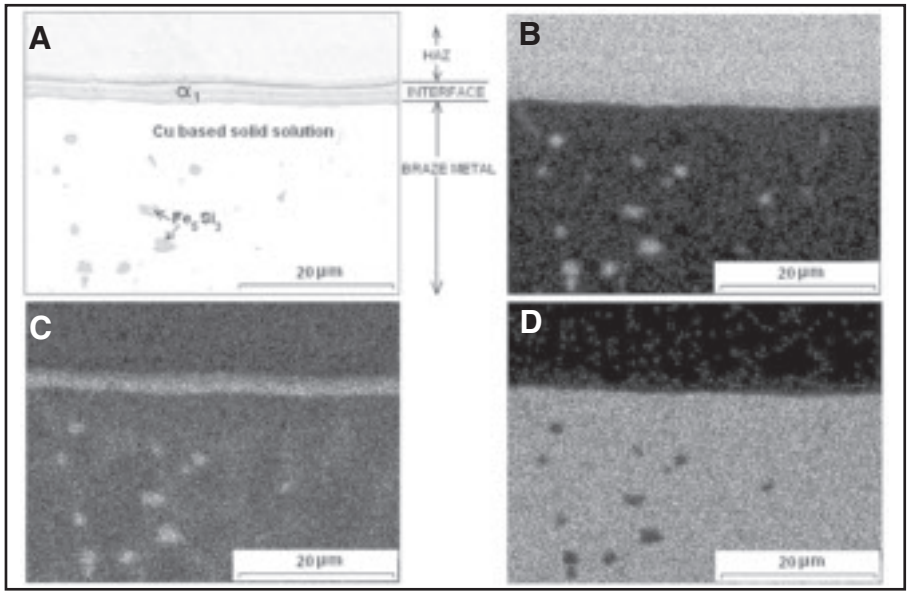

Fig. 5 — EDS elemental mapping of the as-polished joint region of P1. A — FESEM backscattered electron image; B — distribution of iron (Fe Kα); C — distribution of silicon (Si Kα); D — distribution of copper (Cu Kα).

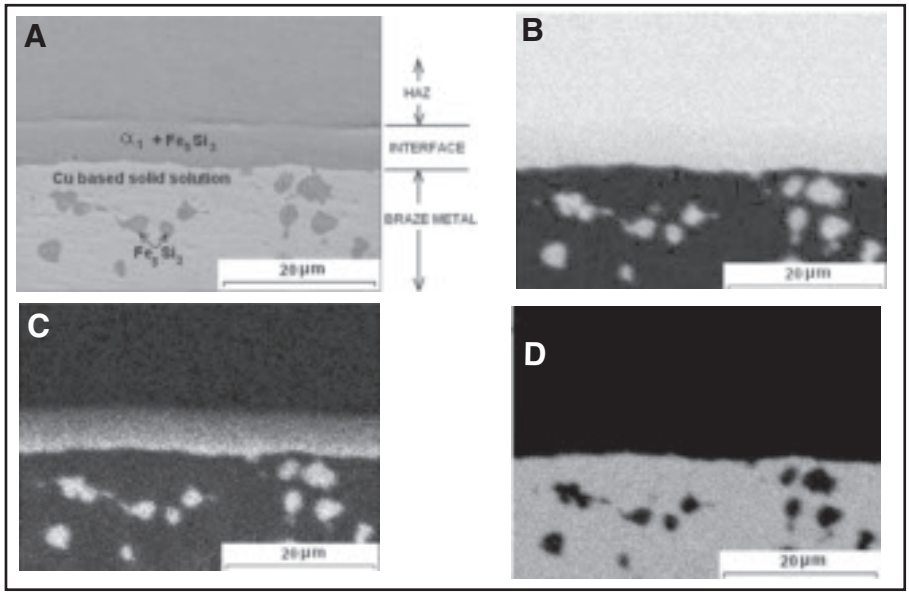

Fig . 6 — EDS elemental mapping of the as-polished joint region of P2. A — FESEM back sscattered electron image; B — distribution of iron (Fe Kα); C — distribution of silicon (Si Kα); D — distribution of copper (Cu Kα).

specimens in etched condition are presented in Fig. 8A and B. These microstructures of HAZ exhibit destroyed polygonal ferrite grains and the presence of acicular ferrite. The equiaxed polygonal grain morphology is mostly destroyed due to thermal cycle experienced by this region. The thermal cycle (temperature-time history) of the joint region during the GMA brazing process is shown in Fig. 9. According to Cu-Si phase diagram (Ref. 12), the solidification range of Cu-3.7 wt-% Si alloy (filler metal) is 940°–1010°C.

During brazing, the joint regions of the specimens, P1 (lower heat input) and P2 (higher heat input), were heated to the maximum recorded temperatures of 1017° and 1184°C, respectively — Fig. 9. These temperatures are higher than the liquidus temperature (1010°C) of the filler metal/electrode and below the solidus temperature of the IF steel (which is close to the melting point of the pure iron, 1539°C, carbon content being very low). Accordingly, the brazing filler metal melts and fills the joint to form braze metal; whereas, the IF steel sheets remain at solid state as per the concept of GMA brazing. However, these maximum temperatures are relatively high and close to the solidus temperature of the IF steel. Furthermore, the average cooling rates calculated from Fig. 9 in the solidification range (940°–1010°C) for P1 and P2 are 108°C s^{-1} and 82°C s^{-1}, respectively. Besides, between 910° and 723°C (expected austen-

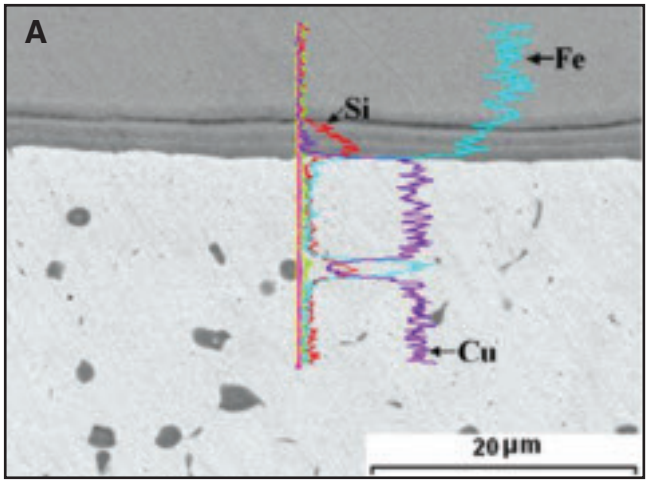

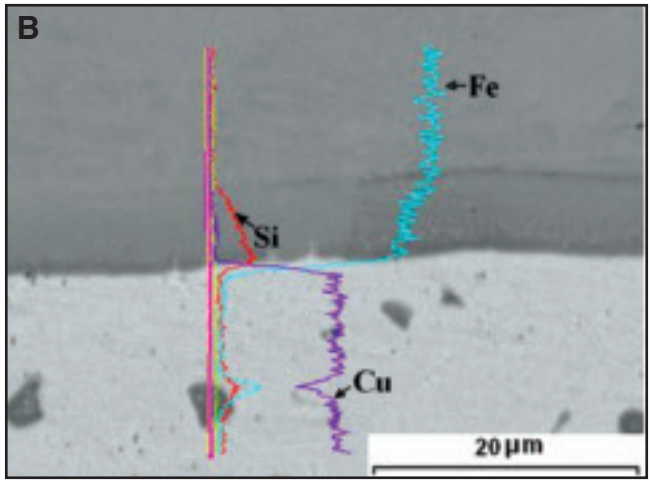

Fig. 7 — EDS line scans at the joint region. A — P1; B — P2.

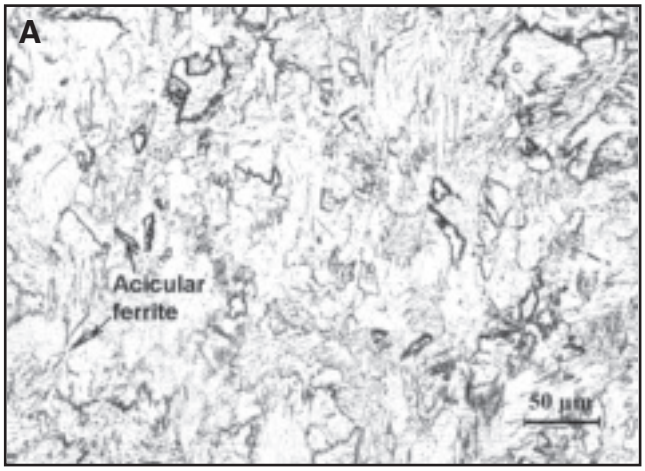

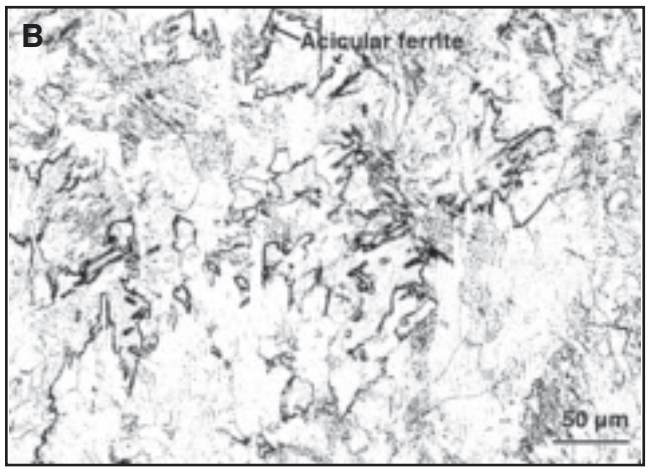

Fig. 8 — Optical microstructures of HAZ: A — P1; B — P2.

ite-to-ferrite transformation regime in HAZ), the calculated average cooling rates for P1 and P2 are 228°C s^{-1} and 133°C s^{-1}, respectively. Therefore, the region of the steel just adjacent to the joint interface (HAZ region) is heated to a high temperature and subsequently subjected to nonequilibrium fast rate of cooling (133°–228°C s^{-1}). The fast rate of cooling is attributed to heat transfer through adjacent base metal that possesses relatively high thermal conductivity. Accordingly, the HAZ region exhibits destroyed polygonal ferrite grains and the presence of acicular ferrite. A rapid cooling from high temperature would result in displacive transformation to generate needlelike acicular ferrite involving para-equilibrium nucleation and diffusionless growth, as also reported elsewhere in low-carbon steel systems (Ref. 13).

The FESEM backscattered electron images and corresponding EDS elemental mapping (Figs. 5, 6) and EDS line scans (Fig. 7) indicate that the interface region is comprised of Fe and Si in both specimens (P1 and P2). The FESEM-based EDS spot analysis carried out within the interface region indicated that the composition range of Si was 9.96–12.47 wt-% in an iron matrix considering both specimens (P1 and P2). According to Fe-Si phase diagram (Fig. 10), at this composition range of silicon, the α_1 phase is stable at room temperature. The α_1 possesses a body-centered cubic (BCC) crystal structure (Ref. 12). The high-resolution bright field TEM images along with selected area diffraction pattern (SADP) of the interface region are presented in Fig. 11A and B. The specimen with low-heat input (P1) exhibits only the presence of BCC α_1 phase at the interface — Fig. 11A. However, the specimen with high heat input (P2) shows the presence of fine round-shaped hexagonal Fe_5Si_3 phase dispersed in BCC α_1 matrix — Fig. 11B. The presence of Fe_5Si_3 could only be properly revealed and identified by selected area diffraction in TEM (about 338 nm in average diameter).

Both specimens (P1 and P2) also contain the hexagonal Fe_5Si_3 phase in the form of patches in the braze metal distributed in the copper-enriched matrix. This is identified by the FESEM backscattered electron images and corresponding EDS elemental mapping (Figs. 5, 6), and the high-resolution TEM images along with SADP analysis — Fig. 12A, B. The FESEM-based EDS spot analysis indicates that the copper-based alloy matrix contained 2.35–3.13 wt-% Si, 0.77–0.89 wt-% Mn, and 3.06–3.29 wt-% Fe for both specimens (P1 and P2). According to graphical point count analysis of the FESEM images, the area fractions occupied by Fe_5Si_3 in braze metal region for low (specimen P1) and high (specimen P2) heat inputs are 4.30% and 14.17%, respectively. Also, the size of the patches of Fe_5Si_3 appears to be larger for the higher heat input braze joint. The result of X-ray diffraction analysis (Fig. 13) of the entire joint region for both specimens (P1 and P2) further confirms the presence of all the phases previously identified, viz. α-iron matrix (in HAZ and base metal), BCC α_1 intermediate phase (at interface region), Fe_5Si_3 (at braze metal for both the heat inputs and at interface region for higher heat input), and copper-based solid solution (at braze metal). The peaks of BCC iron represent the presence of α-iron matrix and α_1 intermediate phase; while

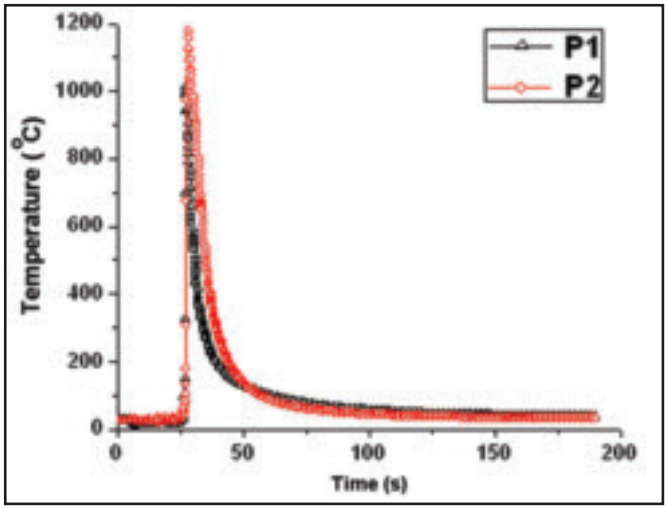

Fig. 9 — The thermal cycle (temperature-time history) of the joint region during GMA brazing process.

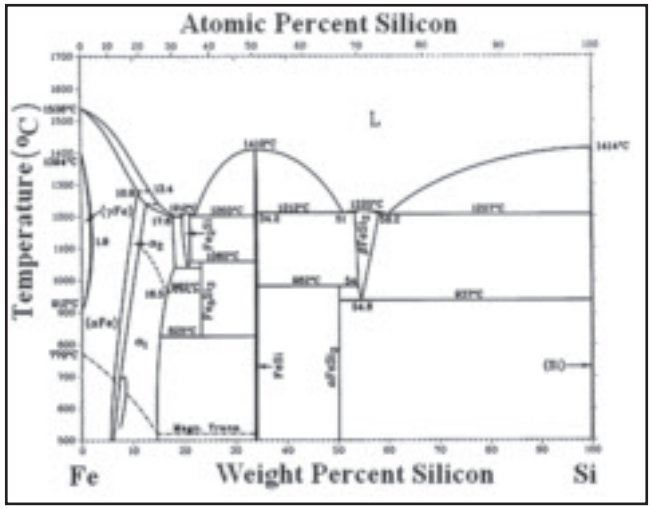

Fig. 10 — Fe-Si phase diagram (Ref. 12).

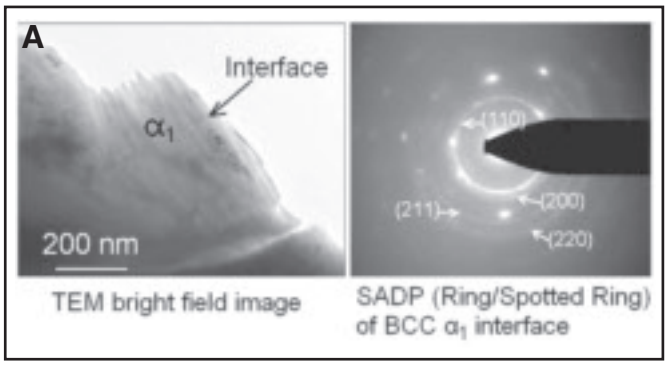

Fig.11 — The high-resolution TEM images along with selected area diffraction pattern (SADP) of the interface region. A — P1; B — P2.

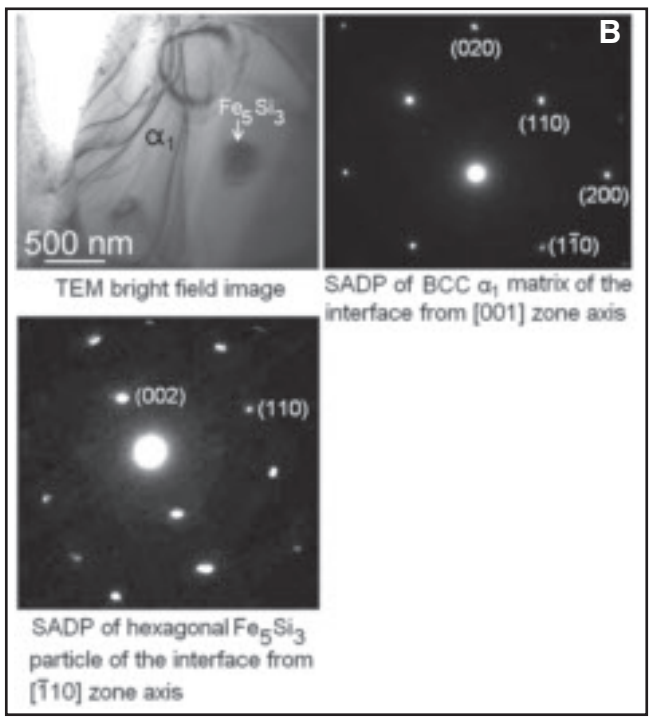

the peaks of copper indicate the existence of copper-based solid solution.

The existence of silicon-enriched, iron-based intermediate phase α_1 at the interface region, and Fe_5Si_3 at the braze metal and at the interface region for higher heat input indicates the diffusion of Fe and Si across the interface of the molten copper-based braze metal (containing Si) and the solid IF steel substrate (containing Fe) at the brazing temperature. Once the molten braze metal (filler metal) fills the joint under capillary action, the silicon present in the molten braze metal diffuses into solid steel generating Si-enriched, ironbased intermediate phase α_1 that forms the interface region. At a higher heat input (specimen P2), the brazing temperature is also higher (1184°C). This accounts for faster diffusion of Si in steel causing the formation of more silicon-enriched phase Fe_5Si_3 of submicron size in a matrix of α_1. Also, the average width of the interface (as measured from FESEM images, Figs. 5, 6) is larger for higher heat input (6.13 μm) than that of the lower heat input (2.15 μm).

According to Batz et al. (Ref. 14), the diffusivity (D in $cm^2\ s^{-1}$) of silicon in α-iron as a function of absolute temperature (T in K) is given as

$$D = 0.44\, e^{-48000/RT} \quad (1)$$

In this relationship, the activation energy (Q) and the frequency factor (D_0) are 48000 Cal mol^{-1} and 0.44 $cm^2\ s^{-1}$, respectively. Taking the value of universal gas constant (R) as 1.986 Cal $mol^{-1}\ K^{-1}$, the diffusivities of Si at two brazing temperatures, viz. 1290 K (1017°C) and 1457 K (1184°C) were calculated as 3.21×10^{-9} $cm^2\ s^{-1}$ (namely, D_1) and 27.49×10^{-9} $cm^2\ s^{-1}$ (namely, D_2), respectively. The diffusion distance (x) is known to be proportional to $(Dt)^{1/2}$ (Ref. 15). By inspection of the heating and cooling cycles for the two heat inputs employed and shown in Fig. 9, the diffusion time (t) may be assumed to be similar in the two cases. Then, the ratio of the diffusion distance (x_2) at 1184°C to the diffusion distance (x_1) at 1017°C would be equal to $(D_2/D_1)^{1/2}$, i.e., 2.93. This value closely matches with the ratio (2.85) of the measured interface width (6.13 μm) at GMA brazing temperature of 1184°C (higher heat input) to the interface width (2.15 μm) at GMA brazing temperature of 1017°C (lower heat input). This clearly indicates that the generation of the thin interface region was a process controlled by the diffusion of silicon in α-iron.

On the other hand, at the brazing tem-

Table 3 — Result of Tensile Shear Test

Sample No.	Maximum Load (kN)	Extension (mm)	Location of Failure
P1	7.13	29.46	Base metal
P2	7.19	28.93	Base metal

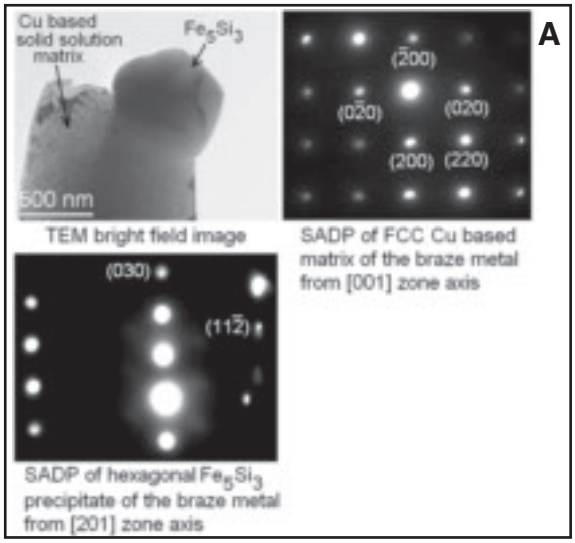

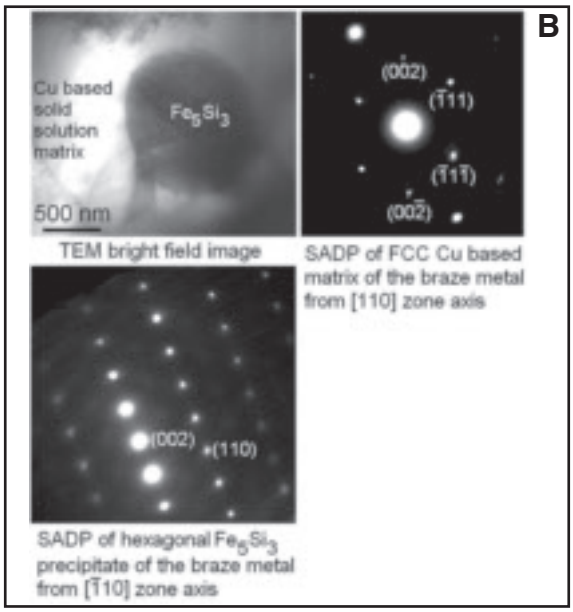

Fig. 12 — The high-resolution TEM images along with selected area diffraction pattern (SADP) of the braze metal region. A — P1; B — P2.

perature, iron diffuses into the molten braze metal and mixes under the arc. During cooling to room temperature, as the copper-based braze metal solidified, iron combined with silicon to form Fe_5Si_3, which comes out as a precipitate in the copper-based matrix.

The relative thermodynamic stability of different compounds of iron and silicon was studied by Zhi-shui et al. (Ref. 16). In the present research work, the data points (Ref. 16) of Gibbs free-energy change (ΔG in kJ mol^{-1}) vs. absolute temperature (T in K) were curve-fitted (using Microsoft Excel software), generating the following relationships:

For FeSi: $\Delta G = 0.0699T - 156.98$, with $R^2 = 0.99$ (2)

For $FeSi_2$: $\Delta G = -0.0117T - 25.901$, with $R^2 = 0.98$ (3)

For Fe_2Si: $\Delta G = 0.0177T - 109.99$, with $R^2 = 0.97$ (4)

For Fe_5Si_3: $\Delta G = 0.0303T - 294.29$, with $R^2 = 0.98$ (5)

The values of coefficient of determination (R^2) very close to 1 represent an excellent accuracy of these equations. Using these equations, the ΔG values at room temperature (300 K) for FeSi, $FeSi_2$, Fe_2Si, and Fe_5Si_3 were calculated as −136.01, −29.41, −104.68, and −285.20 kJ mol^{-1}, respectively. The most negative value of ΔG for Fe_5Si_3 formation as compared to other compounds of Fe and Si justifies the stability of Fe_5Si_3 in the microstructure. The larger volumetric fraction and size of Fe_5Si_3 precipitates in the braze metal at higher heat input (higher brazing temperature) as compared to that at lower heat input (lower brazing temperature) is due to the greater diffusion of Fe in the molten braze metal at a higher brazing temperature (1184°C).

It is important to note that the GMA brazing temperatures (1017° and 1184°C) of the present study exceeded the boiling point of pure zinc (907°C), the coating metal originally present on the galvannealed steel sheets. Therefore, the zinc coating was vaporized locally at the joint region during the GMA brazing process. Subsequently, there was no trace of zinc found in the joint region.

Joint Properties and Joint Efficiency

The microhardness traverse curves for both the specimens (P1 and P2) are shown in Fig. 14. In both the cases, relatively lower hardness is exhibited by the braze metal, as expected for a soft copper-based matrix. At the interface, there is a sharp rise in hardness due to the presence of hard α_1-based matrix. Thereafter, the

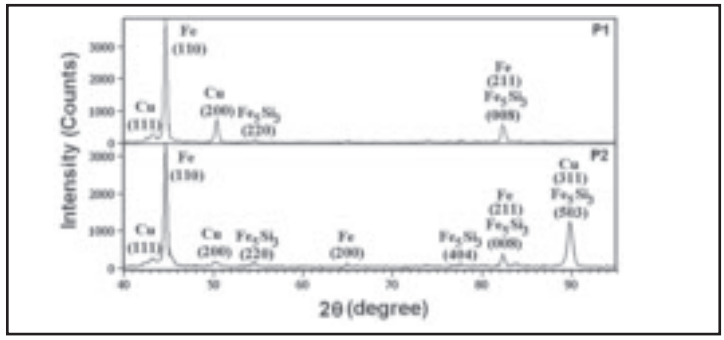

Fig. 13 — X-ray diffraction pattern of the entire joint region.

hardness decreases sharply in the HAZ and base metal. The HAZ region possesses relatively higher hardness than the base metal. The microstructure of the HAZ consists of destroyed polygonal ferrite grains and acicular ferrite. The destroyed polygonal ferrite grain regions appear to be coarser than the ferrite grains of the base metal, though the actual grain size could not be measured due to lack of grain boundary clarity. However, the needle-shaped acicular ferrite possesses a very small crystal size (crystal width in the range of 4–8 μm). Besides, as a displacive transformation product generated through para-equilibrium nucleation and diffusionless growth, acicular ferrite contains a dense substructure of dislocations (Refs. 17–19). However, the polygonal ferrite (as observed in the base metal) is reported to possess significantly lower dislocation content (Ref. 17).

Therefore, due to such morphological and microstructural features, acicular ferrite has been shown to provide not only better hardness and strength, but also higher resistance to crack propagation (Ref. 20). Also, the hardness of the braze metal is marginally higher than the base metal. This is attributed to the presence of uniformly distributed Fe_5Si_3 in the copper-based matrix of the braze metal. While the hardness of the interface region is much higher than the braze metal, HAZ, and base metal in both the specimens, the specimen (P2) with higher heat input exhibits relatively higher hardness (291 HV) of the interface region than the specimen (P1) with lower heat input (268 HV). The interface microstructure of the specimen P1 consists only the α_1 phase. However, the specimen P2 possesses the submicron sized Fe_5Si_3 dispersed in α_1 as the microstructure of the interface region. Accordingly, the additional factor of dispersion hardening contributes to the higher hardness of the interface in specimen P2. In concurrence with the microhardness test results, during tensile shear tests, the failure occurs in the base metal region, the softer and less strong part, indicating 100% joint efficiency. The occurrence of failure from the base metal region

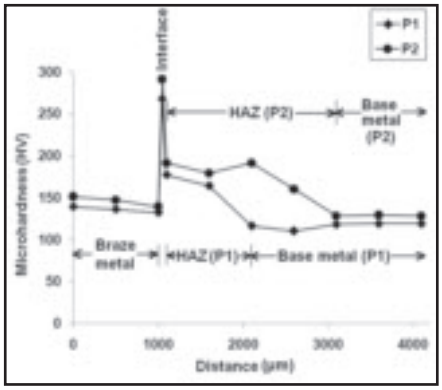

Fig.14 — The microhardness traverse curves of the joint.

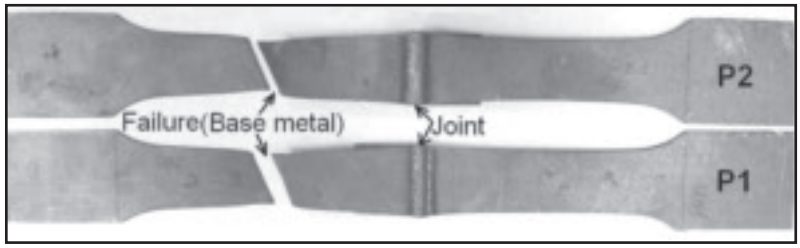

Fig. 15 — The failure location in the GMA brazed specimens subjected to tensile shear loading.

in the specimens subjected to tensile shear loading is shown in Fig. 15. Accordingly, the tensile shear test result (Table 3) exhibits similar maximum load and extension in both specimens (P1 and P2) corresponding to the failure at the base metal region in both the cases. This reflects the much higher hardness (as exhibited in the microhardness test result) and strength of the joint interface than the base metal.

Conclusions

1) The novel method of GMA brazing with Cu-based electrode (filler metal) containing Si produces a hard and strong joint in a galvannealed IF steel through the development of Fe-based, Si-enriched α_1 interface (for lower heat input) or submicron sized Fe_5Si_3 dispersed α_1 interface (for higher heat input).

2) During GMA brazing process, once the molten braze metal (filler metal) fills the joint under capillary action, the silicon present in the molten braze metal diffuses into solid steel forming Si-enriched, iron-based intermediate phase α_1 for lower heat input and dispersed submicroscopic Fe_5Si_3 particles in α_1 matrix for higher heat input that form the interface region.

3) The calculated diffusion distance of Si into the base metal is in excellent agreement with the measured interface width indicating the diffusion of Si in the iron matrix as the controlling factor for evolution of the interface region.

4) At the brazing temperature, iron migrates into the molten braze metal and mixes under the brazing arc. During cooling to the room temperature, as the copper-based braze metal solidifies, iron combines with silicon to form Fe_5Si_3, which comes out as precipitate in the copper-based matrix. The calculated lowest Gibbs free-energy change for the formation of Fe_5Si_3 as compared to other phases of Fe and Si justifies its stability in the microstructure.

5) The presence of acicular ferrite in HAZ and the typical microstructure of Fe_5Si_3 precipitates distributed in copper-based matrix in braze metal provide relatively higher hardness than the base metal. Most importantly, as compared to other regions (base metal, HAZ, and braze metal), a sharp rise in hardness is observed at the interface region that contains α_1 at lower heat input. Still higher hardness of the interface is obtained for higher heat input where submicron-sized Fe_5Si_3 is dispersed in the α_1 matrix. Accordingly, during tensile shear test, failure occurs at the weaker base metal region for both heat inputs, indicating 100% joint efficiency. Therefore, even with a nonferrous copper-based braze alloy (filler metal), it is possible to join IF steel to itself.

Acknowledgment

The authors are thankful to Professor B. S. Murty and Ms. Kanchanamala of Metallurgical & Materials Engineering Department, Indian Institute of Technology Madras, for providing necessary experimental support in transmission electron microscopy.

References

1. Mathis, K., Krajnak, T., Kuzel, R., and Gubicza, J. 2011. Structure and mechanical behaviour of interstitial-free steel processed by equal-channel angular pressing. *Journal of Alloys and Compounds* 509: 3522–3525.

2. Guimaraes, A. S., Mendes, M. T., Costa, H. R. M., Machado, J. D. S., and Kuromoto, N. K. 2007. An evaluation of the behavior of a zinc layer on a galvanized sheet, joined by MIG brazing. *Welding International* 21: 271–278.

3. Chovet, C., and Guiheux, S. 2006. Possibilities offered by MIG and TIG brazing of galvanized ultra high strength steels for automotive applications. *La Metallurgia Italiana* 7–8: 47–54.

4. Iordachescu, D., Quintino, L., Miranda, R., and Pimenta, G. 2006. Influence of shielding gases and process parameters on metal transfer and bead shape in MIG brazed joints of the thin zinc-coated steel plates. *Materials and Design* 27: 381–390.

5. Freytag, N. A. 1965. A comprehensive study of spot welding galvanized steel. *Welding Journal* 44(4): 145-s to 156-s.

6. Howe, P., and Kelley, S. C. 1988. A comparison of the resistance spot weldability of bare, hot-dipped, galvannealed, and electrogalvanized DQSK sheet steels. SAE paper 880280.

7. Upthegrove, W. R., and Key, J. F. 1972. A high-speed photographic analysis of spot welding galvanized steel. *Welding Journal* 51(5): 233-s to 244-s.

8. Gedeon, S. A., and Eagar, T. W. 1986. Resistance spot welding of galvanized steel: Part II, Mechanisms of spot weld nugget formation. *Metallurgical Transactions* B 17B(12): 887–901.

9. Parker, J. D., Williams, N. T., and Holliday, R. J. 1998. Mechanisms of electrode degradation when spot welding coated steels. *Science and Technology of Welding and Joining* 3(2): 65–74.

10. X. Xie. 1997. *Steel Heat Treatment Handbook*, G. E. Totten, M. A. H. Howes (eds.), Marcel Dekker, New York, pp. 986–995.

11. Quintino, L., Pimenta, G., Iordachescu, D., Miranda, R. M., and Pépe, N. V. 2006. MIG brazing of galvanized thin sheet joints for automotive industry. *Materials and Manufacturing Processes* 21: 63–73.

12. Baker, H. (ed.) 1992. *Alloy Phase Diagrams*. *ASM Handbook*, vol 3. ASM International, Materials Park, Ohio, p. 860.

13. Chandrasekharaiah, M. N., Dubben, G., and Kolster, B. H. 1992. An atom probe study of retained austenite in ferritic weld metal. *Welding Journal* 71(7): 247-s to 252-s.

14. Batz, W., Mead, H. W., and Birchenall, C. E. 1952. Diffusion of silicon in iron. *Trans. AIME* 194: 1070.

15. Shewmon, P. G. 1963. *Diffusion in Solids*. McGraw-Hill Book Co., New York, p.13.

16. Zhi-shui, Y. U., Rui-feng, L. I., and Kai, Q. I. 2006. Growth behavior of interfacial compounds in galvanized steel joints with $CuSi_3$ filler under arc brazing. *Transactions of Nonferrous Metals Society of China* 16: 1391–1396.

17. Tang, Z. 2006. Optimizing the transformation and yield to ultimate strength ratio of Nb-Ti micro-alloyed low carbon line pipe steels through alloy and microstructural control. PhD thesis, University of Pretoria, Republic South Africa, pp. 32–182.

18. Zhao, M. C., Yang, K., Xiao, F. R., Shan, Y. Y. 2003. Continuous cooling transformation of undeformed and deformed low carbon pipeline steels. *Mater. Sci. Eng. A* 355: 126–136.

19. Thompson, S. W., Colvin, D. J., and Krauss, G. 1990. Continuous cooling transformations and microstructures in a low-carbon, high-strength low-alloy plate steel. *Metallurgical Transactions A* 21A: 1493–1507.

20. Komizo, Y., and Fukada, Y. 1990. In: Advances in welding metallurgy. *Proceedings from the First United States-Japan Symposium,* American Welding Society, Japan Welding Society, and The Japan Welding Engineering Society, San Francisco, Calif., Yokohama, Japan, pp. 227–250.